Boundary effect in electrorheological fluids

X. L. Gong,[1,*] F. Yang,[1] S. H. Xuan,[1] L. H. Zong,[1] W. Zhu,[2] and W. Q. Jiang[2]

[1]*Department of Modern Mechanics, CAS Key Laboratory of Mechanical Behavior and Design of Materials,*
University of Science and Technology of China (USTC), Hefei 230027, People's Republic of China
[2]*Department of Chemistry, USTC, Hefei 230026, People's Republic of China*

The effect of the boundary friction coefficient on the rheological properties of the electrorheological (ER) fluids in quasistatic and dynamic states is investigated by computer simulation. The relation between the shear stress and the boundary friction coefficient in quasistatic and dynamic states is discussed qualitatively and quantitatively, and the trend matches the previously reported experimental results well. The flow curves of ER fluids, under different friction coefficients, are calculated, and it is found that the friction coefficient affects the flow curves. In two dimensions, the transitions in structure corresponding to the shear stress variations are presented to understand the mechanism of ER fluids.

I. INTRODUCTION

Electrorheological (ER) fluids, typically smart materials, are composed of microsized or nanosized dielectric particles dispersed in a liquid with a low dielectric constant [1–4]. When an electric field is applied, the randomly dispersed particles are rearranged along the field direction and form complex columnlike structures, dramatically changing the apparent viscosity. The change is fast (milliseconds) and is reversible, which makes the ER fluids desirable for technological and industrial applications. During the past decade, various inorganic particles, liquid crystals, and polymers were developed for ER fluids [5,6], and these ER fluids can be applied in clutches, brakes, damping devices, actuators, fuel injection valves, hydraulic valves, and robotic controlling systems [7–9].

Besides the experimental work, theoretical calculations also are very important for the ER fluids [10,11]. To obtain better knowledge of the flow behavior of ER fluids, many theoretical models were developed to discuss the ER phenomenon. First, the electric double layer and water bridge models were developed to discuss the hydrous ER fluids. Then, a polarization model was proposed for anhydrous ER fluids [12]. Hao introduced a dielectric loss model that offers guidance on how to formulate a high performance conventional ER fluid [13]. Wen *et al.* developed the polar molecular model for giant ER fluids [14]. Various parameters, including the electric field strength, the frequency of the electric field, the conductivity, the particle dielectric properties, the particle volume fraction, the temperature, and the water content, are considered. However, most of these papers are focused only on the particle-particle interaction; the particle-boundary interaction has not been considered thoroughly. It has been found that the flow behaviors of both the Newtonian liquid [15] and the non-Newtonian liquid were affected by boundary conditions [16]. As typical non-Newtonian liquids, the ER fluids also would largely be dependent on the boundary conditions. Therefore, more work should be done to clarify the relationship between the shear property of the ER fluids and the boundary conditions.

Recently, a few experiments, which focused on the effect of boundary conditions on the properties of ER and magnetorheological (MR) fluids, were reported. The effect of boundary conditions on the shear behavior is separated into quasistatic and dynamic states. In the quasistatic state, Lemaire and Bossis compared the yield stress of experimental and theoretical results (based on interparticle forces) and found the difference mainly was caused by the surface roughness [16]. Lee and Jwo studied the ER effect with grooved electrode surfaces and found that the denser the rolled grooves on the electrode surfaces, the more the enhanced ER effect [17]. Based on these papers, Zhang *et al.* [18] and Peng *et al.* [19] found that the material that has larger interactions with boundary particles gets greater yield stress. Recently, Wang *et al.* found that the boundary sliding weakens the shear stress of the ER fluids, and this problem could be solved by increasing the roughness of the boundary [20]. As a result, it can be concluded that the increased boundary roughness causes the increased yield stress. In the dynamic state, Hanaoka *et al.* used a metallic net to study surface morphology on the ER effect, and it was shown that an appropriate surface, but not the greatest amount of roughness, was effective for promoting the ER effect [21]. By comparing the experiment between the quasistatic and the dynamic states, it is found that the as-obtained results do not agree with each other. To date, the research on the boundary effect on the ER properties mainly has been experimental testing; no theoretical and computational discussions have been reported. Previously, by using the boundary friction assumption, the trembling shear behavior was studied by our group [22]. Pappas and Klingenberg also conducted a simulation for the MR fluid and found that the boundary friction force affects the lamellar structure formation distinctly [23]. Unfortunately, the reason why the increased friction coefficient yield increased yield stress but not dynamic shear stress still is not clear.

In this paper, a computer simulation was conducted to systematically examine the boundary effect on the properties of ER fluids. The relations between the shear stress and the boundary friction coefficient are discussed qualitatively

---

*gongxl@ustc.edu.cn

and quantitatively, and the tendency matches the previously reported experimental results. The optimum friction coefficient, which can lead to the greatest dynamic shear stress, was obtained by this calculation. To further understand the mechanism of ER fluids in static and dynamic states, the structure transformations corresponding to the stress variation were discussed. Moreover, the charge's relaxation was considered in this simulation.

II. MODEL AND SIMULATION

The ER system, which is simulated in this paper, consists of N spherical particles (the relative dielectric constant is ε_p, and the diameter is σ) suspended in a silicone oil fluid whose relative dielectric constant and viscosity are $\varepsilon_f (\varepsilon_f < \varepsilon_p)$ and η_f, respectively. The tested ER fluid, which is confined between two parallel-plate electrodes, is separated by a distance L_z (Fig. 1). An external electric field is applied perpendicularly to the parallel plate (the z direction), and a steady shear rate $\dot{\gamma}$ is imposed along the x direction (parallel with the plate). Here, the velocity field is varied linearly along the z direction (the top electrode moves at a speed of $\dot{\gamma} L_z$). Because the particles are much larger than the liquid molecule, it is thought that slip happens between the particles and the electrodes but not between the liquid molecules and the electrodes. Before the application of the electric field, particles were randomly dispersed in the medium fluid. When the electric field E_0 is applied along the z direction, each particle gets an induced dipole moment $\mathbf{p} = (1/2)\pi\beta\varepsilon_0\varepsilon_f\sigma^3\mathbf{E}_{\text{loc}}$ in the fluid with relative dielectric constant ε_f (in the Système International unit system) where $\beta = (\varepsilon_p - \varepsilon_f)/(\varepsilon_p + 2\varepsilon_f)$ and $\mathbf{E}_{\text{loc}}$ is the local field, with $\mathbf{E}_{\text{loc}} = E_0\hat{z}$ if $\beta \ll 1$.

In a shear flow of shear rate $\dot{\gamma}$, a spherical sphere spins at an angular velocity of $\omega = \dot{\gamma}/2 (\omega = \omega\hat{y})$ [24]. For the rotating dielectric sphere in an electric field, because of the rotational motion that leads to a displacement of its polarized charges on
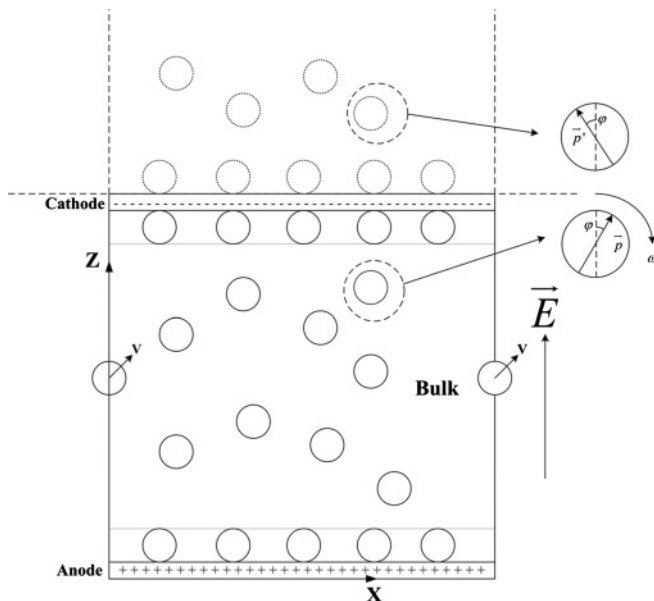

FIG. 1. Schematic of the simulation model.

the surface and the relaxation of the surface charges, the rate of change in the dipole moment is given by [25]

$$d\mathbf{p}/dt = \omega \times \mathbf{p} - (\mathbf{p} - \mathbf{p}_0)/\tau_r. \tag{1}$$

The dipole moment $\mathbf{p} = p_x\hat{x} + p_z\hat{z}$ at the steady state is expressed as

$$p_x = \frac{\omega\tau p_0}{1 + (\omega\tau_r)^2}, \quad p_z = \frac{p_0}{1 + (\omega\tau_r)^2}, \tag{2}$$

where τ_r is the relaxation time. In the rotational state, there is a tilt angle φ between the dipole moment and the z direction and $tg\varphi = \omega\tau_r$. For the rotational particles, the dipolar force acting on the ith particle from the particle at r_j is given by

$$\mathbf{F}_{ij}^{\text{el}} = F_0(\sigma/r_{ij})^4\{[1 - 3\cos^2(\theta_{ij} - \varphi)]\hat{r} - \sin[2(\theta_{ij} - \varphi)]\hat{\theta}\}. \tag{3}$$

where $p = |\mathbf{p}|$, $\mathbf{r}_{ij} = r_i - r_j$ with $r_{ij} = |\mathbf{r}_{ij}|$, θ_{ij} is the angle between $\mathbf{r}_{ij}$ and the z axis, $\hat{r} = \mathbf{r}_{ij}/r_{ij}$, and $F_0 = 3p^2/(4\pi\varepsilon_0\varepsilon_f\sigma^4)$. To simulate interactions between the hard spheres and the interactions between the hard sphere and the hard wall (the two electrodes), an exponential short-range repulsive force between particles i and j is introduced as

$$\mathbf{F}_{ij}^{\text{rep}} = 2F_0(\sigma/r_{ij})^4 \exp[-100(r_{ij}/\sigma - 1)]\hat{r}, \tag{4}$$

and between the particle i and the hard wall,

$$\mathbf{F}_i^{\text{wall}} = 2F_0(\sigma/z_i)^4 \exp[-100(r_{ij}/\sigma - 0.5)]\hat{z} - 2F_0$$
$$\times [\sigma/(L_z - z_i)]^4 \exp\{-100[(L_z - z_i)/\sigma - 0.5]\}\hat{z}. \tag{5}$$

For the boundary particles, the friction force between the boundary particles and the electrodes is introduced as

$$\mathbf{F}_i^{\text{fric}} = \mu N_i, \quad \text{when} \quad N_i > 0,$$
$$\mathbf{F}_i^{\text{fric}} = 0, \quad \text{when} \quad N_i \leq 0. \tag{6}$$

N_i is the normal force acting on the ith boundary particle,

$$N_i = \sum_{j(j\neq i)} \left(\mathbf{F}_{ij}^{\text{el}} + \mathbf{F}_{ij}^{\text{rep}}\right) \cdot \hat{z}, \quad \text{for the cathode,}$$
$$N_i = -\sum_{j(j\neq i)} \left(\mathbf{F}_{ij}^{\text{el}} + \mathbf{F}_{ij}^{\text{rep}}\right) \cdot \hat{z}, \quad \text{for the anode.} \tag{7}$$

The dipolar force acting on the ith particle from the image particle at r_j is given by

$$\mathbf{F}_{ij}^{\text{el},im} = F_0(\sigma/r_{ij})^4\{[\cos 2\varphi - 3$$
$$\times \cos(\theta_{ij} - \varphi)\cos(\theta_{ij} + \varphi)]\hat{r} - \sin 2\theta_{ij}\hat{\theta}\}. \tag{8}$$

Then, the forces acting on the ith particles are

$$\mathbf{F}_i = \sum_{j(j\neq i)} \left(\mathbf{F}_{ij}^{\text{el}} + \mathbf{F}_{ij}^{\text{rep}}\right) + \sum_j \mathbf{F}_{ij}^{\text{el},im} + \mathbf{F}_i^{\text{wall}} + \mathbf{F}_i^{\text{fric}},$$
$$\text{for boundary particles,} \tag{9}$$

$$\mathbf{F}_i = \sum_{j(j\neq i)} \left(\mathbf{F}_{ij}^{\text{el}} + \mathbf{F}_{ij}^{\text{rep}}\right) + \sum_j \mathbf{F}_{ij}^{\text{el},im} + \mathbf{F}_i^{\text{wall}}, \quad \text{for the others.}$$

The motion of the ith particle is described by [26]

$$m\, d^2\mathbf{r}_i/dt^2 = \mathbf{F}_i - 3\pi\sigma\eta_f (d\mathbf{r}_i/dt - \dot{\gamma} z_i\hat{x}) + \mathbf{R}_i, \tag{10}$$

where m is the mass of particles and $\mathbf{r}_i$ is the position of the ith particle at time t. The first term $\mathbf{F}_i$ is the interparticle force, the second is the Stokes drag, and the third is the Brownian force. The Brownian force $\mathbf{R}_i$ is determined independently by a normal distribution with $\langle R_{i,\alpha} \rangle = 0$ and $\langle R_{i,\alpha}(0) R_{i,\beta}(t) \rangle = 6\pi k_B T \sigma \eta_f \delta_{\alpha\beta} \delta(t)$. k_B is the Boltzmann constant, and T is the absolute temperature. To study the parametric properties of many different ER fluids, we define dimensionless quantities to scale Eq. (1): $\mathbf{r}_i^* = \mathbf{r}_i/\sigma$, $t^* = t/[3\pi\eta_f\sigma^3/(k_B T)]$, $\mathbf{R}_i^* = \mathbf{R}_i/(k_B T/\sigma)$ and $\mathbf{F}_i^* = \mathbf{F}_i/[p^2/(\varepsilon_0\varepsilon_f\sigma^4)]$, so Eq. (1) can be rewritten as

$$A\, d^2\mathbf{r}_i^*/dt^{*2} = Q\mathbf{F}_i^* - d\mathbf{r}_i^*/dt^* + 8\,\mathrm{Pe}\, z_i^* \hat{x} + \mathbf{R}_i^*, \quad (11)$$

where $Q = p^2/(\varepsilon_0\varepsilon_f\sigma^3 k_B T)$ and $\mathrm{Pe} = 3\pi\eta_f\sigma^3\dot{\gamma}/(8k_B T)$. For the ER fluids, the magnitude of $A = mk_B T/(3\pi\eta_f\sigma^2)^2$ in Eq. (6) is very small ($\sim 10^{-10}$), so this inertial effect is neglected in the following simulations. Thus, it is simplified as

$$d\mathbf{r}_i^*/dt^* = Q\mathbf{F}_i^* + 8\,\mathrm{Pe}\, z_i^*\hat{x} + \mathbf{R}_i^*. \quad (12)$$

Equation (7) is integrated with a time step $\Delta t^* \leqslant 0.01/(F_{\max}^* Q)$ using Euler's method; $F_{\max}^*$ is the dimensionless maximum interparticle force that acts on particles, thus, the maximum displacement of particles cannot exceed 0.01σ.

In this paper, a system of $N = 240$ particles (20 stick to the top electrode, and 20 stick to the bottom electrode) in a box with $L_x = 15\sigma$, $L_y = 5\sigma$, and $L_z = 15\sigma$ is simulated. The particle volume fraction is 0.11. Periodic boundary conditions are imposed in the x and y directions, reflecting boundary conditions in the z direction.

In the dynamic state, rheological properties are determined by the effective viscosity η_{eff}, which can be calculated from the stress $\tau_{zx}(\eta_{\mathrm{eff}} = \langle\tau_{zx}\rangle/\dot{\gamma})\tau_{zx}$ is the zx component of the stress tensor, which is an averaged value of the simulations. By using the Bingham model, τ_{zx} is expressed as $\tau_{zx} = \tau_E + \eta_s\dot{\gamma}$, where η_s is the viscosity of suspensions (without an electric field). In order to definitely understand the relationship of the particle interactions, we focused on the electric field induced shear stress τ_E, which was calculated by Eq. (14) [27],

$$\tau_E = \left\langle -\frac{1}{V}\sum_{i=1}^{N}(\mathbf{r}_i)_z\left(\mathbf{F}_i^{\mathrm{el}}\right)_x\right\rangle. \quad (13)$$

The dimensionless shear stress is defined as $\tau^* = \tau/\tau_s$ and $\tau_s = 3/16\pi\varepsilon_0\varepsilon_f\beta^2 E_0^2$.

III. RESULTS AND DISCUSSION

Three-dimensional simulations were carried out in a box ($15 \times 5 \times 15$) with parameters as follows: $T = 300$ K, $\varepsilon_p = 100$, $\varepsilon_f = 2$, $\sigma = 5$ μm, $\eta_f = 0.1$ Pa s. Our simulation is conducted under a lamellar flow, and the relation between the shear stress and the friction coefficient is studied. About the boundary effect, Pappas and Klingenberg have studied the effect of friction force on the velocity distribution [21]. Our paper is a supplement about the research on the boundary effect.

Figure 2 shows the relation between the relative shear stress and the shear strain under different friction coefficients. It is observed that the pre-yield process is not obvious when
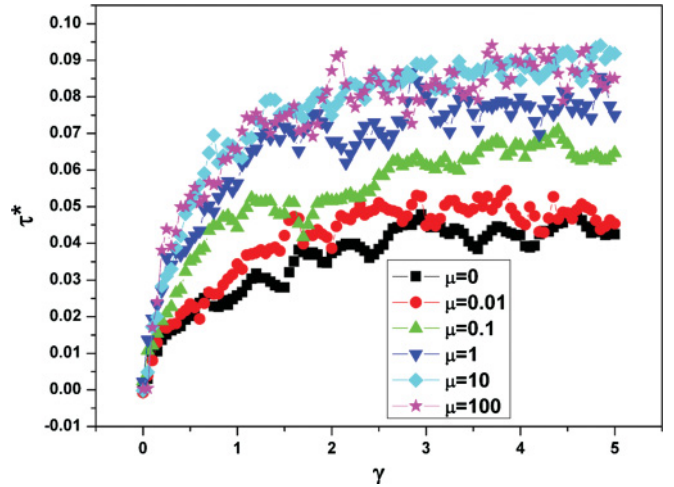

FIG. 2. (Color online) Relative shear stress vs strain under different friction factors in the quasistatic state. $\dot{\gamma} = 0.001$ s^{-1}, $\tau_r = 10^{-5}$ s, and $E = 1200$ V/mm.

the friction coefficient is small. It means that the solid state of the ER fluid with the electric field applied does not appear when small friction coefficient electrodes are used. However, the larger friction coefficients show a very obvious pre-yield process, and the increased friction coefficient leads to a greater yield stress until the friction coefficient $\mu = 10$. Peng et al. measured the yield stress of the MR fluids with the boundary friction coefficients 0.1 and 0.4 and found that the boundary friction coefficient 0.4 yielded greater yield stress [19]. This result also agrees with the other previously reported experimental results [16–18].

Under the dynamic shear flow, the relation between the stress and the friction coefficient is different from the quasistatic state. Figure 3 shows the relations between the shear stress and the friction coefficient under different shear rates and electric fields. When $\mu = 0.01$, the friction coefficient is too small so that great slip occurs between the electrodes and the boundary particles. In this case, the shear stress is caused mainly by the viscous force, thus, it nearly remains constant (Fig. 4, when $\mu = 0.01$). When the friction coefficient increases, the friction force acting on the boundary particles increases, and the shear stress increases. However, the shear stress decreases when the friction coefficient comes to a critical value. Here, nearly no slip happens between the electrodes and the boundary particles. The structures totally appear as destruction and reformation that correspond to the shear stress going up and down with the strain as shown in Fig. 4 (when $\mu = 50$). So, the average shear stress on large friction coefficients becomes small. Also, it is found that the greatest shear stress exists in the middle section (from $\mu = 0.3$ to 6, probably). In this section, the boundary particles are not totally in the slip and no-slip situations. As shown in Fig. 4, when $\mu = 2$, the boundary friction force balances with the viscous force. In this state, the shear stress is the greatest. It is observed that the shear stress is nearly constant with only a little vibration. This means that the structures are stable in this state. Based on the above discussion, two conclusions of the relation between the stress and the friction coefficient at quasistatic and dynamic states can be achieved. The first one
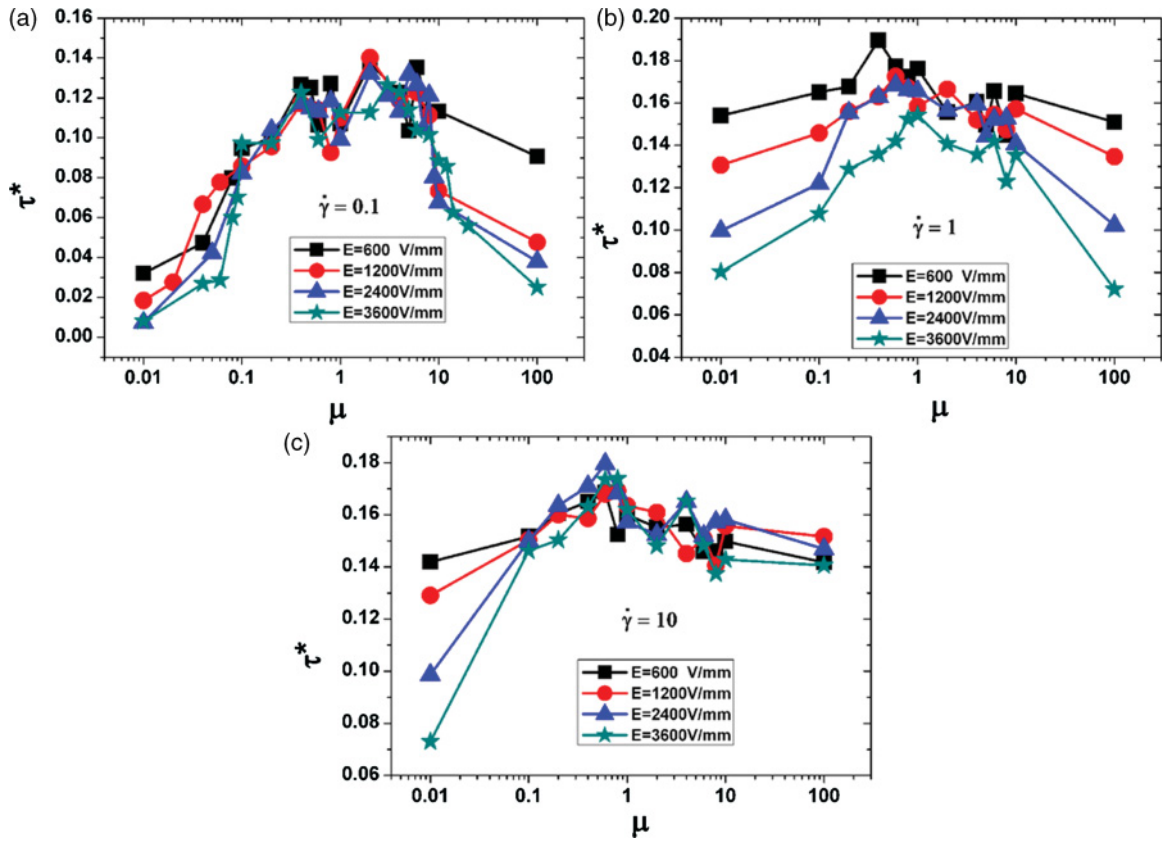
FIG. 3. (Color online) Relative shear stress vs friction factor under different electric fields and shear rates.

is that the yield stress increases with the friction coefficient until the friction coefficient is large enough. For the second, the shear stress increases with the friction coefficient at the small friction coefficient section and decreases with the friction coefficient at the large friction coefficient section, and the greatest shear stress is in the middle section, which also can be supported by the previous experimental results conducted by Hanaoka *et al.* [21].They measured the shear stress with the boundary covered with a metallic net and found that, not the tenser and sparser mesh size, but a middle proper mesh size can yield the greatest shear stress.

In order to get the flow curve, the shear stresses τ were calculated with a series of shear rates from 0.01 to 100 s^{-1}. The shear rate increases step by step, and each shear stress date at a certain shear rate in Fig. 5 is calculated separately. The data are obtained by calculating the average relative shear stress at a given electric field and shear rate (as shown in Fig. 4). It is found that different boundary conditions show different rheological properties. In the small shear rate region (shear rate from 0.01 to 1 s^{-1}), the effect of the boundary friction coefficient is more obvious than in the other regions. Too small or too large a friction coefficient cannot lead to great shear stress in this region. In the middle region (shear rate from 1 to 10 s^{-1}), the relative shear stress under four different friction coefficients is similar to each other. However, the greatest relative shear stress is found when the friction coefficient is 0.4. The greatest shear stress is shown in this region because the friction force and the viscous force become parallel; the chains have the largest tilt angle. Finally, in the large shear rate

region (shear rate greater than 10 s^{-1}), the relative shear stress drops with increasing the shear rate. This result indicates that the chain structures are totally destructed.

In order to understand the relations between the rheological properties and the structures transformation, the simulations also are conducted in a two-dimensional (2D) situation. The simulations are conducted in a box (15×15), and the simulations are started when several perfect chains are formed
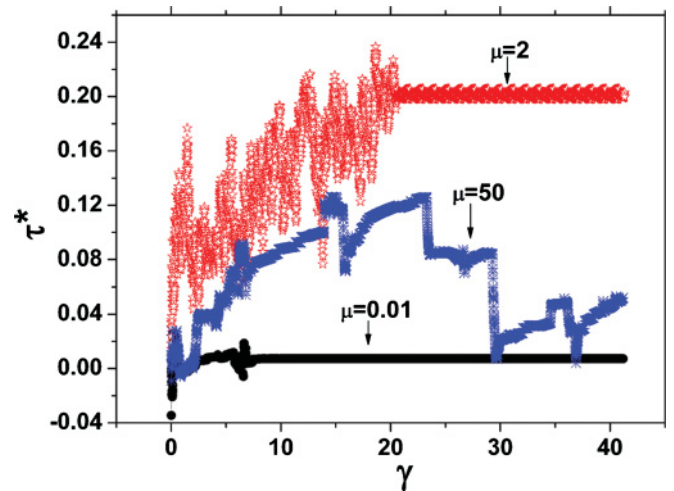

FIG. 4. (Color online) Relative shear stress vs strain under different friction factors in the dynamic state. $\dot{\gamma} = 0.01$ s^{-1}, $\tau_r = 10^{-5}$ s, and $E = 2400$ V/mm.
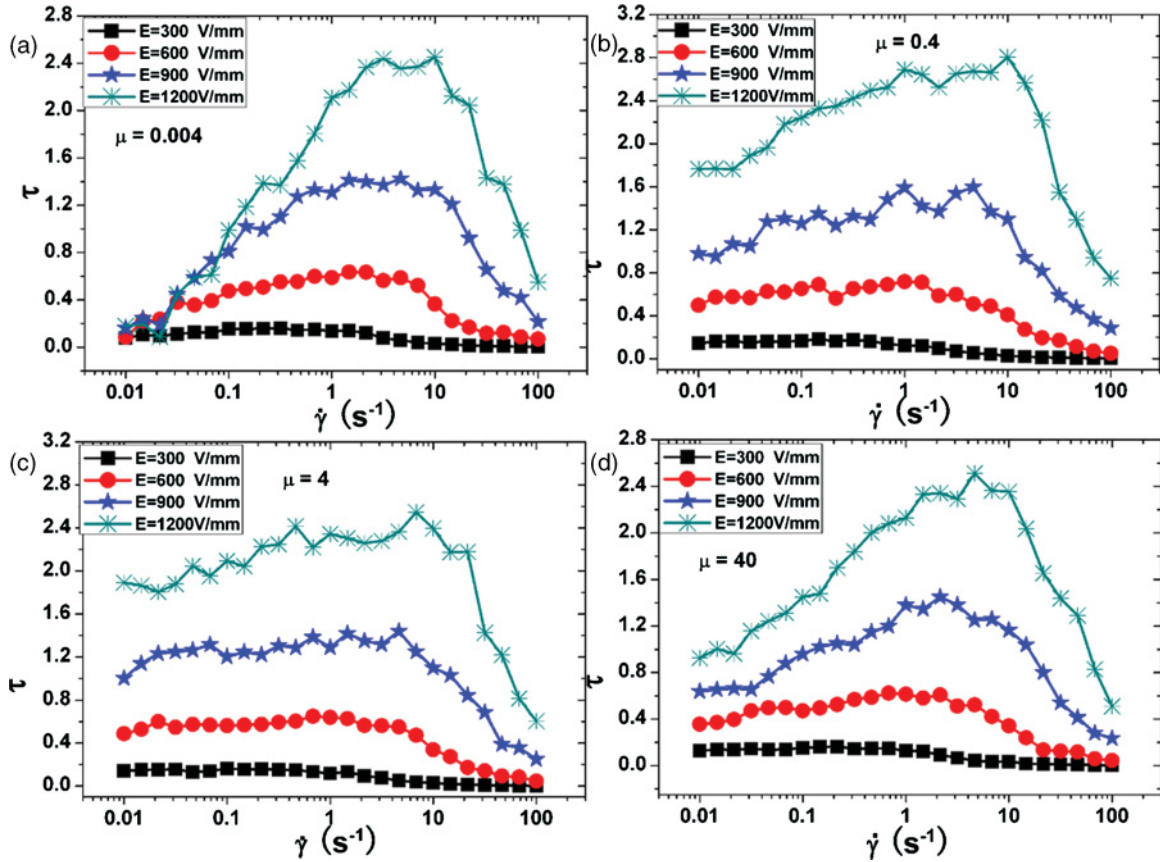
FIG. 5. (Color online) The simulation results of flow curves under different friction coefficients.

and this is an ideal simulation. Figure 6 shows the relation between the relative shear stress and the strain in the quasistatic state. In Fig. 6(a) ($\dot{\gamma} = 10^{-15}$ s^{-1}), when $\mu = 0, 0.04, 0.4$, the yield stress increases with the friction coefficient, whereas, when $\mu = 10^{40}$, the stress appears to be different. It is because, when the friction coefficient is small ($\mu = 0, 0.04, 0.4$), the yield is caused by the boundary slip. Slip happens between the electrodes and the chains at the yield point, and the chains are not broken. When the friction coefficient is large enough ($\mu = 10^{40}$), the structure's destruction is the reason for the yield in the ER effect. However, when the shear rate gets larger [Figs. 6(b) and 6(c)], the flow curves appear to be different. The structure's destruction does not happen in Figs. 6(a) and 6(c) when $\mu = 10^{40}$. It is because, when the shear rate becomes larger, the chain tilt angle becomes larger, and the chains are in the stretched state. So, the normal force is zero, and then, the friction force is zero. A slip happens between the electrodes and the chains in this state. Compared with the simulation results conducted in three dimensions, the structure's destruction [in Fig. 6(a)] and the intact structure's slip along the electrodes [in Figs. 6(a) and 6(b)] coexist in real situations.

Figure 7 shows that the structure transforms with time at different concentrations and shear rates in the dynamic shear state. Under a relatively small shear rate, intact tilted chains slip along the electrode. When the shear rate is increased to a moderate value, the structures are relatively intact and just experience a little destruction and reformation. It is found that

the structures are affected greatly by the viscous force. Thus, under the large shear rate, the particles next to the electrodes are still in the chain structure, while the middle particles totally are disordered. This phenomenon has already been observed by Klingenberg and Zukoski [28]. Figure 8 is the relative shear stress vs the strain relation and the corresponding structure transformation. x stress is the x component of the stress tensor, and the shear is in the x direction, so x stress is the shear stress. z stress is the z component of the stress tensor. The top normal stress is the pressure stress that the boundary particles act on the top electrode, and the bottom normal stress is that on the bottom electrode. The structure transformation can be separated into four regions. Region I corresponds to the D → E process. In structure D, the shear stress is the greatest, the chain tilt angle is the largest, and the chains remain intact. In the D → E process, chains stretch along the chain direction, and the interval between particles becomes too large that the chain structures experience destruction. In this process, x stress decreases, and the normal stress nearly is zero because chains are stretching. Region I is the structure destruction region. Then, the structure experiences region II, the reformation process (from E → G). In region II, the normal stress increases. As shown in Fig. 8, a chain could be thought to be a rod. In the A → D process, the rod rotates clockwise and stretches (the particle interval becomes large). Then, in the E → G process, the rod rotates anticlockwise. If a long tilted rod transforms into a short vertical rod, pressure acts on the electrodes, so the normal stress increases in region II.
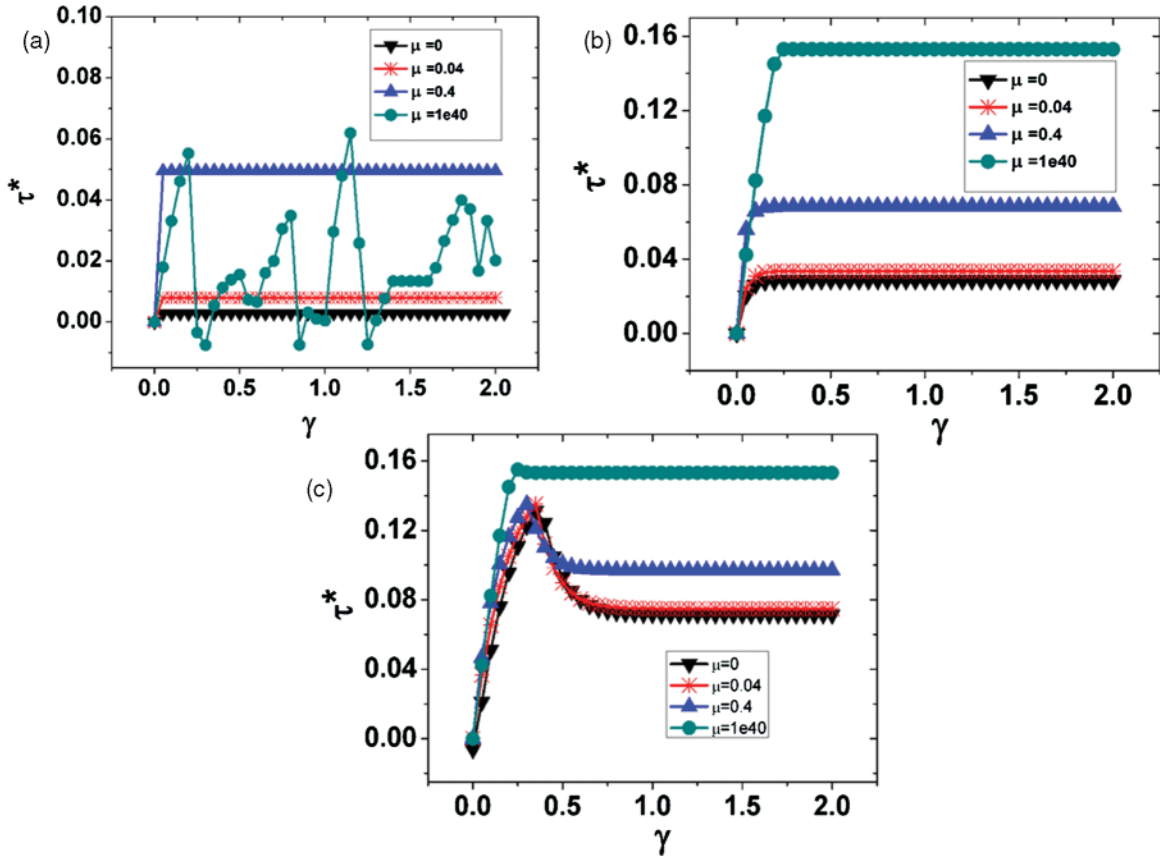
FIG. 6. (Color online) Two-dimensional simulation results of the relative shear stress vs the strain with three chains. $E = 300$ V/mm, $\tau_r = 10^{-5}$, and $\dot{\gamma} = 10^{-5}, 10^{-4}, 10^{-3}$ s^{-1} separately.
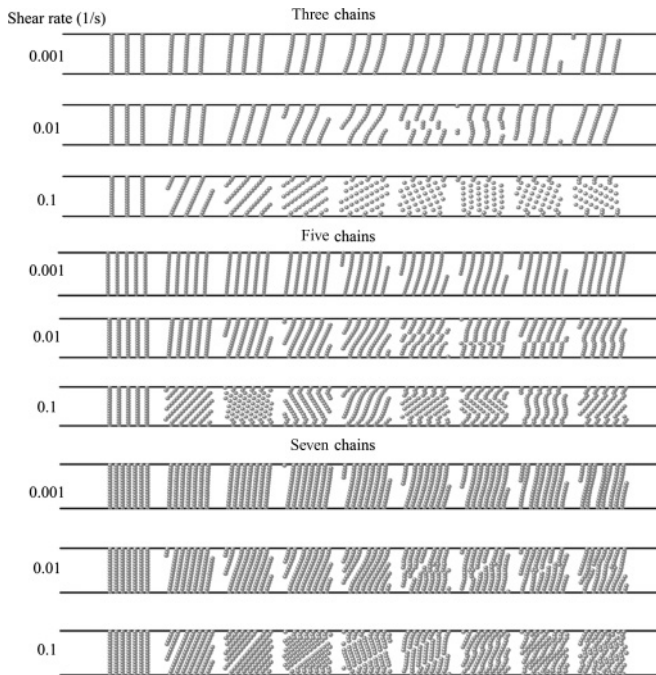

FIG. 7. Configurations of 2D suspensions at long times and different concentrations. The bottom electrode is fixed, and the top electrode shears to the right at shear rates of 0.001, 0.01, and 0.1 s^{-1}. $E = 300$ V/mm and $\mu = 0.4$.

Region III begins with the smallest x stress and ends with the greatest z stress (G $\rightarrow$ H process). If the chains are vertical (such as in structure A), it is thought that the two states (the x stress is the smallest, and the z stress is the greatest) should coexist. But in region III, the two states do not coexist. This phenomenon is caused by the fine adjustment of the particle
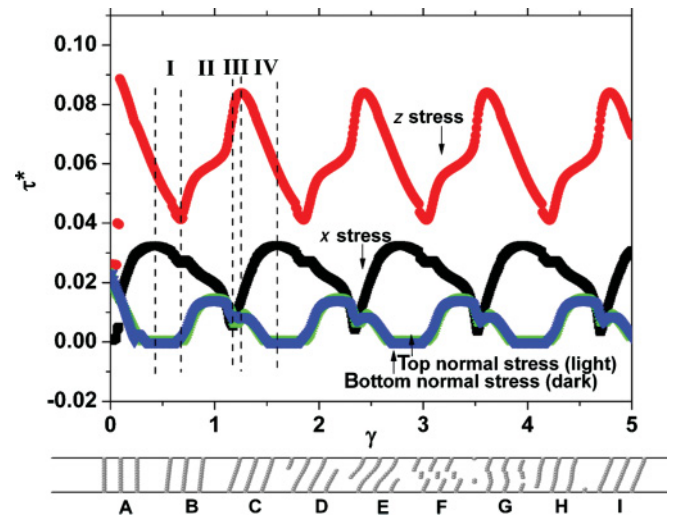

FIG. 8. (Color online) Two-dimensional simulation results of the relative shear stress vs the strain with three chains. $E = 300$ V/mm, $\tau_r = 10^{-5}$, and $\dot{\gamma} = 0.01$ s^{-1}.

interval. Region IV is a chain tilt region where chains tilt in the shear direction from structure H → I. The particle interval becomes large, and the chains are kept intact. Therefore, the shear stress increases, and the z stress and the normal stress decrease.

IV. CONCLUSIONS

The effect of the boundary friction coefficient on the rheological properties of the ER fluids is investigated by simulating the properties at quasistatic and dynamic states. The results match the experimental results reported by other researchers. In the quasistatic state, the yield stress increases with the boundary friction coefficient until the friction coefficient is large enough. While in the dynamic state, the shear stress first increases with the friction coefficient and then decreases with the friction coefficient. A section of the friction coefficient exists where the greatest shear stress is obtained. The flow curves of the ER fluids, under different friction coefficients, are calculated, and it is found that the friction coefficient affects the flow curves. That may afford the possibility to design a boundary for the needed flow properties. An ideal 2D simulation is conducted to observe the relations between the rheological properties and the structure transformation. The above paper will be useful for understanding the mechanism of ER fluids.

[1] T. C. Halsey, Science **258**, 761 (1992).

[2] W. J. Wen, X. X. Huang, S. H. Yang, K. Q. Lu, and P. Sheng, Nature Mater. **2**, 727 (2003).

[3] W. Q. Jiang, C. X. Jiang, X. L. Gong, and Z. Zhang, J. Sol-Gel Sci. Technol. **52**, 8 (2009).

[4] W. Q. Jiang, W. Zhu, C. X. Jiang, X. P. Zhang, S. H. Xuan, X. L. Gong, and Z. Zhang, Smart Mater. Struct. **20**, 065002 (2011).

[5] T. Hao, Adv. Colloid Interface Sci. **97**, 1 (2002).

[6] H. J. Choi and M. S. Jhon, Soft Matter **5**, 1562 (2009).

[7] R. Tao and J. M. Sun, Phys. Rev. Lett. **67**, 398 (1991).

[8] J. R. Melrose, Phys. Rev. A **44**, R4789 (1991).

[9] *Proceedings of Ninth International Conference on Electrorheological Fluids and Magnetorheological Suspensions*, edited by K. Q. Lu, R. Shen, and J. X. Liu (World Scientific, Singapore, 2004).

[10] D. J. Klingenberg, F. van Swol, and C. F. Zukoski, J. Chem. Phys. **91**, 7888 (1989).

[11] B. Wang, Y. L. Liu, and Z. M. Xiao, Int. J. Eng. Sci. **39**, 453 (2001).

[12] M. Parthasarathy and D. J. Klingenberg, Mater. Sci. Eng. R **17**, 57 (1996).

[13] T. Hao, Appl. Phys. Lett. **70**, 1956 (1997).

[14] W. J. Wen, X. X. Huang, and P. Sheng, Soft Matter **4**, 200 (2008).

[15] C. Neto, D. R. Evans, E. Bonaccurso, H. J. Butt, and V. S. J. Craig, Rep. Prog. Phys. **68**, 2859 (2005).

[16] E. Lemaire and G. Bossis, J. Phys. D: Appl. Phys. **24**, 1473 (1991).

[17] C. Y. Lee and K. L. Jwo, Mater. Des. **22**, 277 (2001).

[18] X. Z. Zhang, X. L. Gong, and P. Q. Zhang, J. Appl. Phys. **96**, 2359 (2004).

[19] X. Q. Peng, F. Shi, and Y. F. Dai, Int. J. Mater. Prod. Technol. **31**, 27 (2008).

[20] X. Z. Wang, R. Shen, D. Wang, Y. Lu, and K. Q. Lu, Mater. Des. **30**, 4529 (2009).

[21] R. Hanaoka, M. Murakumo, H. Anzai, and K. Sakurai, IEEE Trans. Dielectr. Electr. Insul. **9**, 10 (2002).

[22] F. Yang, X. L. Gong, S. H. Xuan, W. Q. Jiang, C. X. Jiang, and Z. Zhang, Phys. Rev. E **84**, 011504 (2011).

[23] Y. Pappas and D. J. Klingenberg, Rheol. Acta **45**, 621 (2006).

[24] U. M. Dassanayake, S. S. R. Offner, and Y. Hu, Phys. Rev. E, **69**, 021507 (2004).

[25] J. T. K. Wan, K. W. Yu, and G. Q. Gu, Phys. Rev. E **62**, 6846 (2000).

[26] H. X. Guo, Z. H. Mai, and H. H. Tian, Phys. Rev. E **53**, 3823 (1996).

[27] Z. H. Sun, X. X. Wang, A. K. Soh, and H. A. Wu, Modell. Simul. Mater. Sci. Eng. **14**, 423 (2006).

[28] D. J. Klingenberg and C. F. Zukoski IV, Langmuir **6**, 15 (1990).